Climatic Change (2013) 118:213–226
DOI 10.1007/s10584-012-0632-0

Hydro-climatic effects of future land-cover/land-use change in montane mainland southeast Asia

Omer L. Sen · Deniz Bozkurt · John B. Vogler · Jefferson Fox · Thomas W. Giambelluca · Alan D. Ziegler

Received: 23 August 2010 / Accepted: 11 November 2012 / Published online: 24 November 2012

Abstract Regional climate model simulations with RegCM3 were performed to investigate how future land-cover/land-use (LCLU) change in Montane Mainland Southeast Asia (MMSEA) could affect regional climate. Simulation land-surface parameterizations included present day and plausible 2050 land-covers, as well as two extreme deforestation simulations. In the simulations, the original land cover map of RegCM3, based on AVHRR 1992–93 observations, was replaced with one obtained from MODIS 2001 observations; and the model was set to work at two different spatial resolutions using the sub-grid feature of the land surface model: 27.79 km for the atmosphere and 9.26 km for the land surface. During validation, modeled precipitation closely matched observed precipitation over southern China, but underestimated precipitation in the Indochina Peninsula. The plausible 2050 LCLU simulation predicted little change in regional climate. However, an extreme irrigated crop parameterization caused precipitation to increase slightly in the Indochina Peninsula, decrease substantially in southeastern China, and increase significantly in the South China Sea. The extreme short-grass parameterization caused substantial precipitation decreases in MMSEA, but few changes elsewhere. These simulations indicate in order for significant

Electronic supplementary material The online version of this article (doi:10.1007/s10584-012-0632-0) contains supplementary material, which is available to authorized users.

O. L. Sen (✉) · D. Bozkurt
Eurasia Institute of Earth Sciences, Istanbul Technical University, Istanbul, Turkey
e-mail: senomer@itu.edu.tr

J. B. Vogler
Center for Applied GIS, University of North Carolina, Charlotte, NC, USA

J. Fox
East West Center, Honolulu, HI, USA

T. W. Giambelluca
Geography Department, University of Hawai'i at Mānoa, Honolulu, HI, USA

A. D. Ziegler
Geography Department, National University of Singapore, Singapore, Singapore

climatological changes to occur, substantially more LCLU conversion is required than the 16 % change we incorporated into the plausible 2050 land-cover scenario.

1 Introduction

Terrestrial land cover is an important component of the coupled climate system (Foley et al. 1998). Land-cover change worldwide over the last several decades is thought to have contributed to climatic perturbations at various scales by altering water and energy fluxes and through the emission of greenhouse gases to the atmosphere, primarily through biomass burning and decomposition (Karl and Trenberth 2003). Much attention has been given to the climatic implications of rapid and expansive forest conversion in tropical areas (FAO 2010). Tropical forests, which cover an area of approximately 800 million hectares, are being cleared at an annual rate of about 14 million hectares (Pielke et al. 2007). Between 1990 and 2010, the Indochina Peninsula (IP) lost about 8 % of its forest cover (FAO 2010). Much of the past deforestation took place in lowland areas in the Southeast Asia region (i.e., below 500 m). In recent years, however, many upland areas have undergone extensive land-cover change (Fox et al. 2012).

Montane Mainland Southeast Asia (MMSEA, Fig. 1b) has come under close scrutiny as a result of deforestation, land degradation, and most recently, the conversion of traditional agricultural practices to more permanent cash crop agriculture systems (Fox et al. 2012). The MMSEA region is poised for additional LCLU changes, stimulated in part by the expansion of international highway networks and plantation agriculture, particularly rubber (Ziegler et al. 2009a; Fox et al. 2012). Fox et al. (2012) estimate that these activities, along with emerging regional and international markets for cash crops, will help drive a 16 % change in the landscape over the first 50 years of the 21st century. Their model-based projections suggest (a) increases in diversified crop farming, mixed farming, tea and rubber plantations, deciduous broadleaf trees and evergreen shrubs, and urban and other built-up areas; and (b) decreases in evergreen broadleaf trees, mixed forests, forest/field mosaics and tall grass.

Not only do human-induced LCLU changes have important implications for biodiversity, catchment hydrology, carbon sequestration, and local-scale climate phenomena (e.g., Giambelluca et al. 2003; Guardiola-Claramonte et al. 2010; Ziegler et al. 2009b), extensive forest conversion in Southeast Asia may also affect regional and continental-scale climate (e.g., Kanae et al. 2001; Sen et al. 2004; Werth and Avissar 2005; Schneck and Mosbrugger 2011). For example, a significant decrease in rainfall during the height of the summer monsoon rainy season is thought to have already occurred over IP as a result of extensive deforestation in lowland areas (Kanae et al. 2001). Werth and Avissar (2005) simulated significant local reductions in precipitation in Southeast Asia in response to deforestation. Schneck and Mosbrugger (2011) simulated remote as well as local changes in climate as a result of deforestation in Southeast Asia. They report that, despite reductions in precipitation on the deforested grid cells, enhanced moisture convergence increased regional precipitation. Simulations by Sen et al. (2004) suggest that past deforestation has far-reaching effects on the East Asian summer monsoon, including significant changes in rainfall over southern China.

As land cover primarily determines surface properties such as surface albedo and roughness length (Schneck and Mosbrugger 2011), human-induced land-cover changes can alter surface energy fluxes, which in turn affect surface-to-atmosphere heat and moisture transport, thereby influencing atmospheric temperature and humidity. Alteration of moist static energy within convective boundary layer can yield changes in local rainfall (Segal et

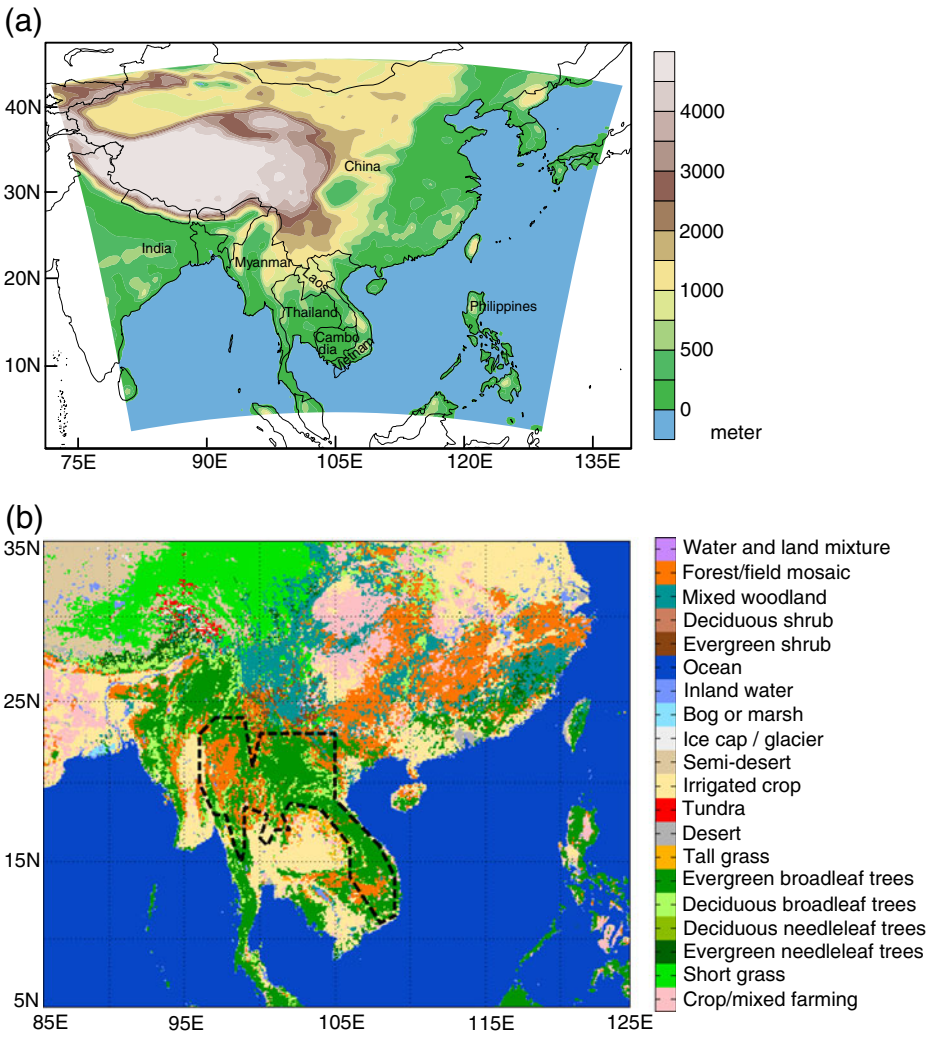

Fig. 1 Domain and topography (at 27.79 km resolution) used in the simulations (**a**), and LCLU map (at 9.26 km resolution) used in the reference simulation (**b**). *Dashed line* delineates Montane Mainland SE Asia

al. 1998). In general, the nature and extension of land-cover change, location and season, determine how landscape change affects local rainfall (cf. Pielke et al. 2007). Remote effects are usually related with the transport of geopotential changes over the conversion area by the large-scale winds (Werth and Avissar 2005). In case of the deforestation in IP, the resulting additional moisture and heat that are carried by the strong monsoonal flow could have played a role in the simulated rainfall changes in the downwind sea and land areas (Sen et al. 2004).

As MMSEA is the headwaters for several major river systems, anthropogenic-induced changes in rainfall would not only have a great effect in the uplands, but also in the lowlands of mainland Southeast Asia. Prediction of regional climatic change over the next half century is useful for developing climate change mitigation/adaptation strategies. We contribute to this effort by simulating the effects of different LCLU change scenarios, including

a realistic projection of the 2050 MMSEA land cover and two extreme cases of deforestation. The results of future climate change predictions based on a high emissions scenario are reported elsewhere (Sen et al. 2012).

2 Methods

The regional climate model (RegCM3) of the International Centre for Theoretical Physics is a primitive equation, hydrostatic, compressible, limited-area model that employs a sigma-pressure vertical coordinate system (Pal et al. 2007). RegCM3 includes the Biosphere-Atmosphere Transfer Scheme (BATS; Dickinson et al. 1993) soil-vegetation-atmosphere model, the non-local boundary layer scheme of Holtslag et al. (1990), the radiative transfer package of the Community Climate Model (CCM3; Kiehl et al. 1996), the ocean surface flux parameterization of Zeng et al. (1998), a simplified version of the explicit moisture scheme of Hsie et al. (1984), and a large-scale cloud and precipitation scheme that accounts for subgrid-scale cloud variability (Pal et al. 2000). Amongst available cumulus cloud schemes, we used that of Grell (1993). The model employs a mosaic-type parameterization of subgrid-scale heterogeneity in topography and land use (Giorgi et al. 2003).

The modeling experiment to investigate climatic effects of LCLU change in MMSEA included the following sets of simulations:

1. Control simulations with a 2001 MMSEA baseline LCLU;
2. Sensitivity simulations with projected LCLU in MMSEA for year 2050 (Fox et al. 2012);
3. Sensitivity simulations featuring the replacement of MMSEA LCLU with irrigated crops class;
4. Sensitivity simulations featuring the replacement of MMSEA LCLU with the short grass.

Each set consists of multi-year simulations performed over the wet periods (between April 15 and October 30) of the years from 1998 to 2002. All analyses are based on the (5-year) averages of the simulation outputs. Figure 1a shows the model domain and topography. The model was run at two different spatial resolutions: 27.79 km for the atmosphere; 9.26 km for the land surface. Thus, one atmospheric grid is coupled to 9 land surface grids, thereby increasing the representativeness of the fine-scale land-surface parameterization. Spatially, 201×171 grid cells were defined for the atmosphere; 603×513 grid cells for the land surface. Eighteen sigma levels represented the atmosphere vertically.

For the baseline land-surface cover we replaced model default land cover (based on AVHRR 1992–93 observations) with MODIS 2001 observations (available in the International Geosphere-Biosphere Programme (IGBP) LCLU classification scheme) translated into the BATS classification scheme. This required up-scaling 0.00833-degree (~0.926 km) MODIS data to a 0.0833-degree (~9.26 km) resolution using the dominant cover approach (model default), then translating IGBP classes to BATS classes (Code is given in Online Resource 1). In some cases AVHRR observations were needed to reassign the classes (e.g., to convert from the IGBP grass class to either the tall or short grass BATS classes). The resulting BATS LCLU map (Fig. 1b) was used in the control simulation.

In the second set of simulations, land-cover was based on projected 2050 MMSEA LCLU map, determined by Fox et al. (2012) using an agent-based model. Using the same rules described above to obtain a baseline BATS LCLU map, their LCLU change simulations were based on historical LCLU transitions and expert knowledge of probable trajectories of change in the region (Fox et al. 2012). The simulations forecast a 16 % change in baseline

vegetation (summarized above). For the extreme scenario experiments, we replaced the MMSEA LCLU with two BATS classes, irrigated crop and short grass. The former was used to represent deforested areas in IP in a prior experiment by Sen et al. (2004). However, the fact that MMSEA is a mountainous region with elevation greater than 500 m makes wholesale conversion to irrigated crops unlikely. Therefore, the short-grass scenario was used to bracket the realm of hydrometeorological effects caused by extreme LCLU change.

Table 1 lists key parameter values of four common land surface covers in the MMSEA region. Simulation initial and boundary conditions were derived from NCEP/NCAR reanalysis data. Sea surface temperatures (SST) were interpolated to model grids from 1-degree Reynolds SST data. BATS initializes soil moisture fields based on grid-cell vegetation and soil types (depth of soil * field capacity * porosity). This paper focuses primarily on the summer season (i.e., June, July and August). The first one and a half month of the simulations (i.e., April and May) is therefore assumed as "spin-up" period. In the monthly plots of area-averaged variables, however, we choose to illustrate the results of all months, excluding only April.

3 Results

3.1 Model performance

Model performance was assessed based on its ability to simulate precipitation in both tropical and mid-latitude areas. Figure 2a and b shows June, July, and August (JJA) precipitation distributions from the gridded CPC Merged Analysis of Precipitation (CMAP, Xie and Arkin 1997) and a regional data set prepared by Yatagai et al. (2012) (hereafter called APHRO data). The general features of the JJA rainfall distribution in Southeast Asia include two regions with high rainfall, one in the Bay of Bengal extending into land areas to the north and east, and the other in the eastern South China Sea. There are two areas where JJA rainfall is lower than their surroundings: the eastern tip and the western interior part of IP. There are disparities between CMAP and APHRO data over land; the most important differences are those along the western coasts and in the northeastern parts of IP where the APHRO data show higher rainfall totals ($\leq$ 33 mm/day along the western coasts and $\leq$18 mm/day in the northeastern parts). The spatial correlation between CMAP and APHRO data was 0.66 for all the land areas.

Overall, the simulated patterns of the precipitation in southeastern Asia (Fig. 2c) agree with observations. However, RegCM3 estimates high JJA precipitation in the Bay of Bengal and along the surrounding coastline, with the greatest rates (24–30 mm day^{-1}) occurring on the western coast of Myanmar. Also, for some locations along the southern and eastern edges of the Tibetan Plateau, simulated precipitation is elevated. The model estimates relatively

Table 1 Parameter values for subset of BATS vegetation types found in MMSEA region

	Short grass	Deciduous broadleaf	Evergreen broadleaf	Irrigated crop
Roughness length (m)	0.05	0.80	2.00	0.06
Minimum stomatal resistance (s/m)	60	120	60	45
Range of LAI (m^2/m^2)	0.5–2	1–6	5–6	0.5–6
Vegetation albedo for λ<0.7 μm	0.10	0.08	0.04	0.08
Vegetation albedo for λ<0.7 μm	0.30	0.28	0.20	0.28

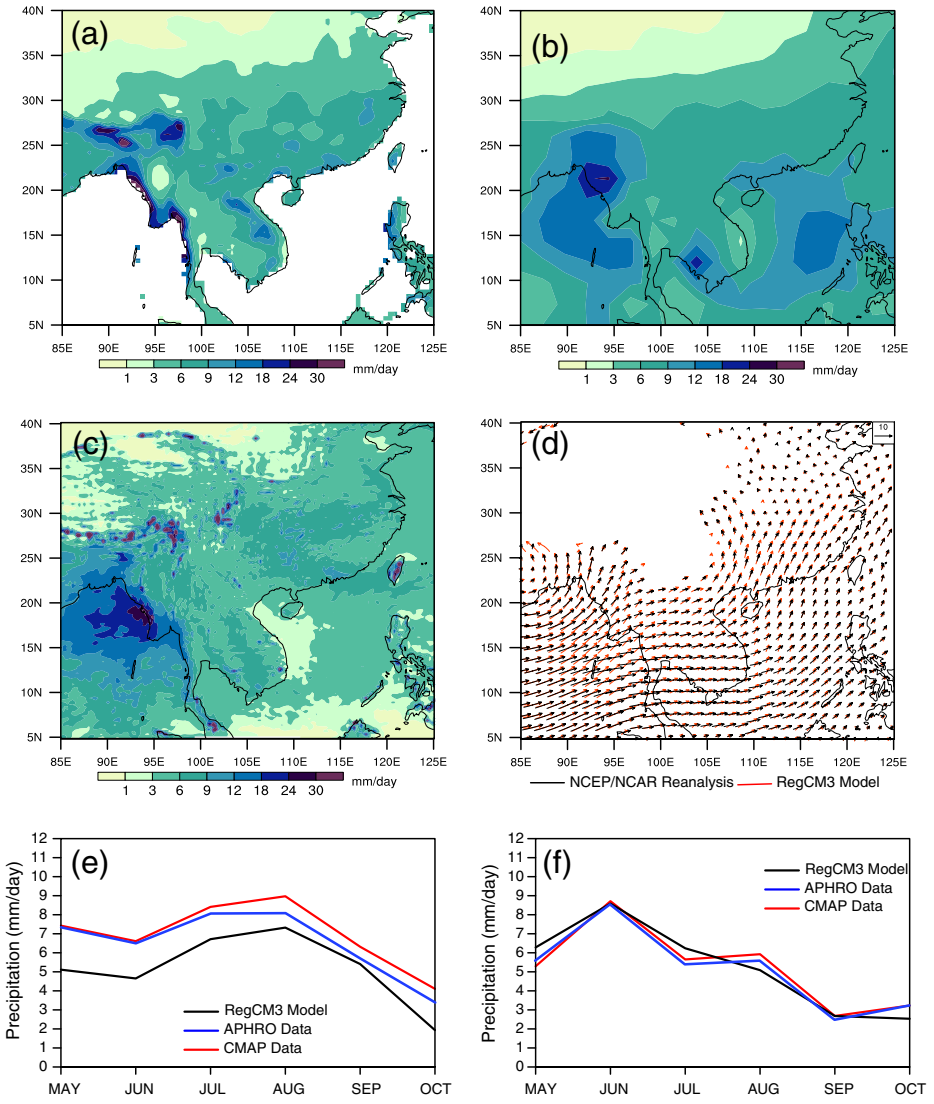

Fig. 2 5-year (1998–2002) mean JJA precipitation from the (**a**) 0.5° APHRO data, **b** 2.5° CMAP data, and (**c**) reference simulation; **d** JJA 850-hPa winds from NCEP/NCAR reanalysis data and the reference simulation; monthly observed and modeled precipitation for (**e**) a box (18–23 N & 96–105 E) covering the northern MMSEA; and (**f**) a box (26–32 N & 105–122 E) covering part of southern China

low precipitation (3–9 mm day^{-1}) for the eastern interior parts of IP. It may also underestimate precipitation for the western sections of the South China Sea. For the land areas shown in Fig. 2, the average and spatial standard deviation of the rainfall estimated by the model (6.99 mm and 4.78 mm, respectively) agree well with APHRO data (7.14 mm and 4.74 mm, respectively), but the spatial correlation between modeled and observed rainfall is relatively low (0.46).

The model reproduced the 850 hPa-level wind circulation reasonably well (Fig. 2d). The major differences occur over eastern parts of Bay of Bengal, western parts of IP and southern

parts of South China Sea where the modeled winds are more southerly, and over southern China where the modeled winds are stronger than NCEP/NCAR reanalysis winds. The more southerly winds over Bay of Bengal could mean (a) more moisture transport northeastward, resulting in more precipitation in the northern parts of Bay of Bengal and adjacent coastal areas to the northeast; and (b) less moisture transport eastward, resulting in less precipitation in IP, South China Sea and southern China.

The observational data indicate that the northern section of MMSEA receives much of the precipitation in summer months, with a peak in August (Fig. 2e). Southern China also receives much of the precipitation in summer months, but the peak occurs in June (Fig. 2f). Note that, especially in the northern MMSEA, some noteworthy differences between the CMAP and APHRO observations exist despite their broad agreement: e.g., APHRO precipitation is lower in July through October. The model underestimates precipitation in the northern MMSEA, however it reproduces the seasonal cycle correctly. The modeled precipitation in southern China matches well with the APHRO and CMAP observations. It should be mentioned that the observation network for the relatively high-altitude locations of IP is sparse, and therefore, the CMAP and APHRO data may not adequately represent actual precipitation in these areas. Nevertheless, the bias in the modeled precipitation is substantial. However this is not uncommon for the regional climate modeling and climate change studies for Southeast Asia (cf. Werth and Avissar 2005; Chow et al. 2006; Chen et al. 2011; Chotamonsak et al. 2011). The modeling studies with RegCM3 that focus on China also report biases in the estimated precipitation (e.g., Zhang et al. 2008; Gao et al. 2012). Castro et al. (2005) state that the model domain size, grid spacing and parameterizations (especially convective schemes) significantly affect the simulated precipitation. The complex topography is also thought to adversely influence the performance of the models for Southeast Asia (Chen et al. 2011). Wang et al. (2004) suggest that, when a large domain is used, model deficiencies could lead to degradation in the simulation of large-scale fields (see Online Resource 2 for more information). The domain in the present study is taken large to include both IP and southern China to be able to detect possible downwind effects of LCLU change in MMSEA. The large domain size could be, therefore, a factor causing the biases in the precipitation simulations. The skill of the cumulus parameterization of the model could be another factor. It is probably more important than the other factors for Southeast Asia (Wang et al. 2003; Sen et al. 2004). Although we tested different cumulus parameterization schemes available in RegCM3, none improved rainfall estimations significantly. Climate change and sensitivity studies report comparative differences (i.e., the differences between future or sensitivity simulations from the current or control simulations) to eliminate some of the uncertainties and biases that are inherent in the models. Therefore, despite the precipitation biases in our simulations that are mentioned above, we deemed the model performance adequate for assessing comparative changes between the control and sensitivity simulations featuring alternative LCLU scenarios.

3.2 LCLU simulations

The projected 2050 LCLU changes (Fig. 1b) include transitions from one woody plant class to another (e.g., from “evergreen broadleaf trees” to “deciduous broadleaf trees”). These transitions represent changes from forest to tree-plantation crops, including rubber (Fox et al. 2012). While the land-cover classes have different parameterizations (Table 1), the extent of the LCLU change is not sufficient to produce large changes in local or regional precipitation

(Fig. 3b). Simulated 2050 precipitation changes over MMSEA, IP, and southern China are usually less than 10 %. However, some small patches, for example in northern Vietnam and central southern China, had greater changes.

The extreme perturbation simulations delineate the maximum potential impact of LCLU change on regional climate. For example, the predicted response to replacing the current land cover with irrigated crops is precipitation decreases in southern China and parts of Vietnam,

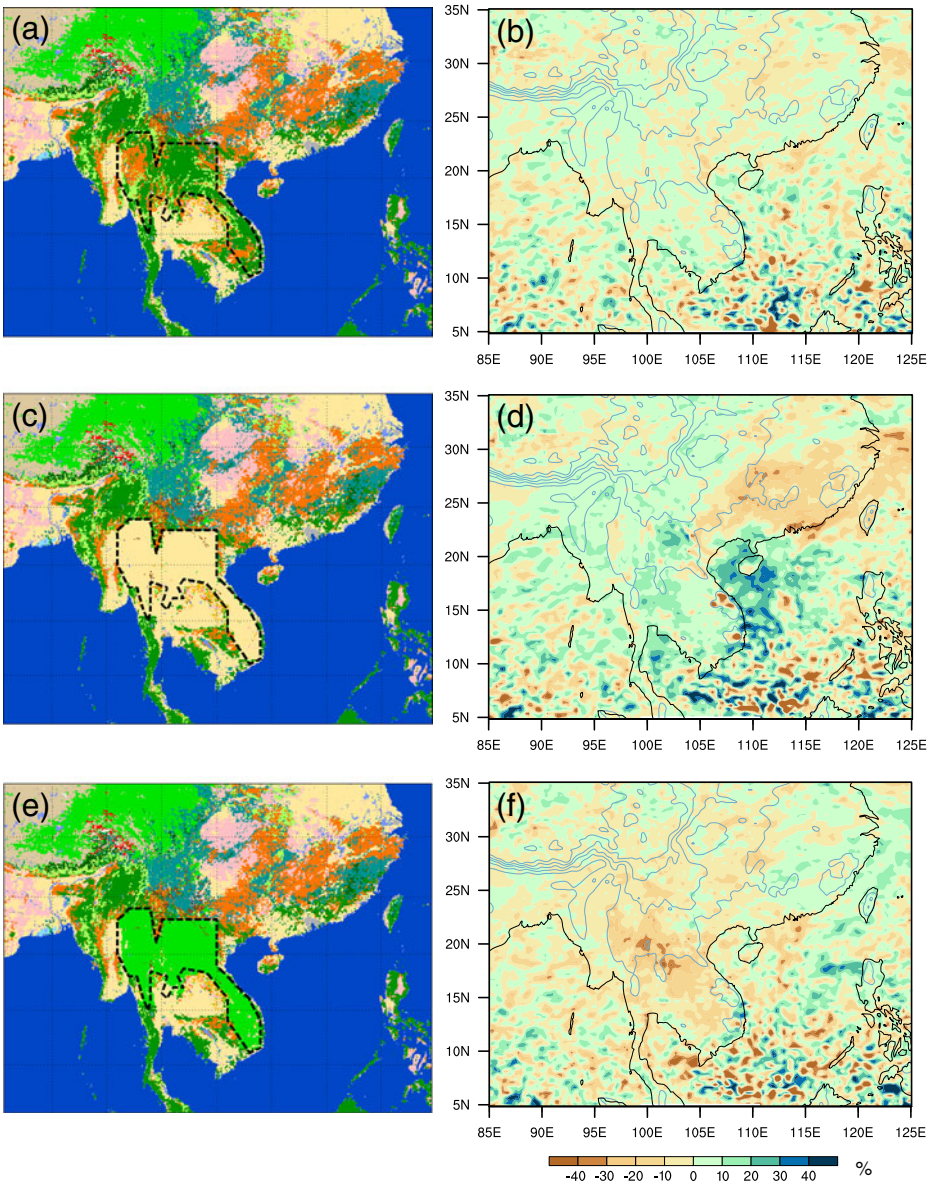

Fig. 3 Maps (at 9.26 km resolution) of projected 2050 LCLU (**a**), irrigated crop scenario (**c**) and short grass scenario and the respective plots (**b**, **d** and **f**) showing the relative changes (%) in JJA precipitation of these experiments

and a general increase throughout most of IP (Fig. 3d). The most striking effects occur downstream of MMSEA. Coherent areas of increased and decreased precipitation occur in the South China Sea and southern China, respectively. These changes are generally >20 %– but the changes are >30 % in some areas. In the extreme short-grass simulation, precipitation reduced over the entire peninsula, with areas in northern MMSEA experiencing reductions ≥30 %.

The projected 2050 LCLU scenario produces small increases in July and October rainfall in northern MMSEA (Fig. 4a). The October increase is nearly 5 % (Fig. 4b). The other

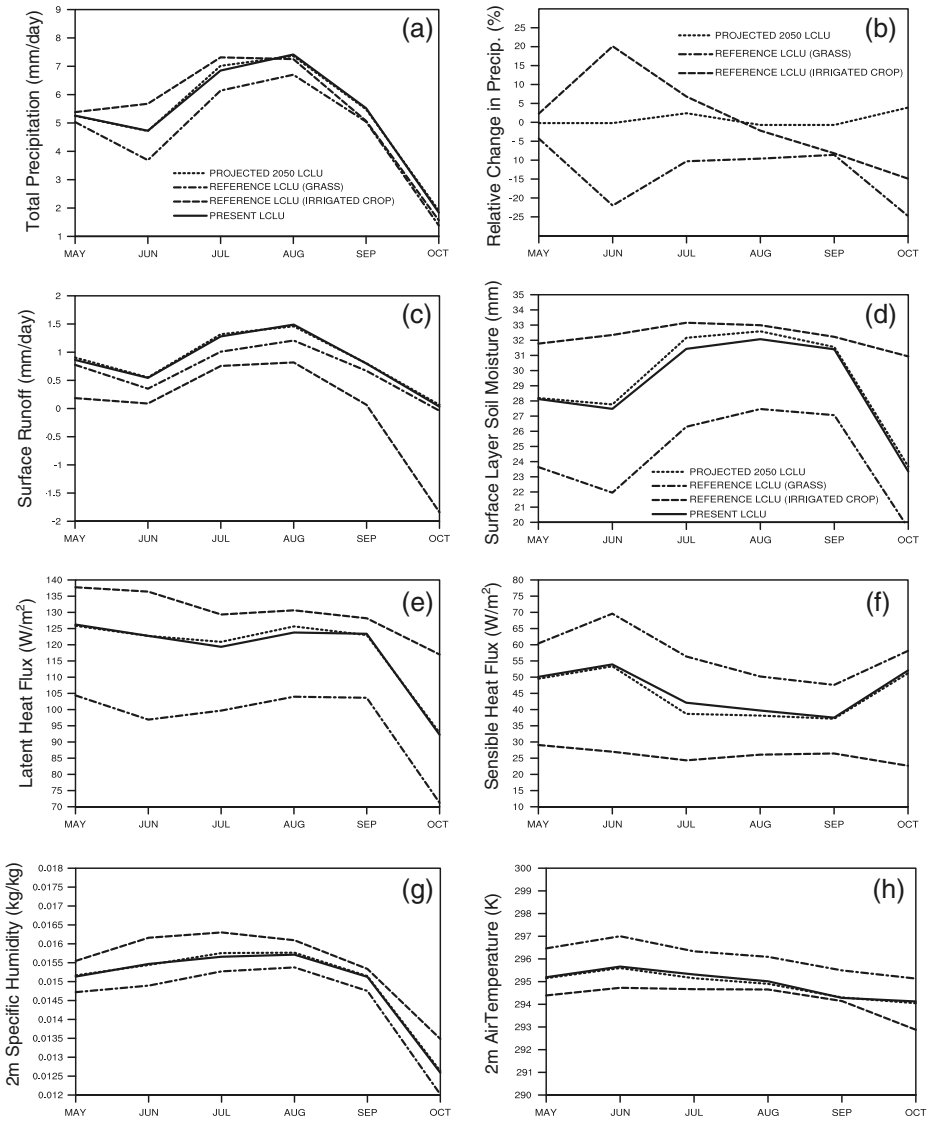

Fig. 4 Modeled monthly precipitation (**a**), the associated relative changes (**b**), surface runoff (**c**), surface layer soil moisture (**d**), latent heat flux (**e**), sensible heat flux (**f**), 2-m specific humidity (**g**), and 2-m air temperature (**h**) for northern MMSEA (18–23 N & 96–105 E)

months do not exhibit outstanding changes. In contrast, the irrigated crop simulation yielded increases from May-July, but reductions in the other months; and the short-grass simulation resulted in reductions in all months. The relative changes in July for both simulations were >20 %. The relative reductions in October are about 15 % and 25 % for irrigated-crop and short-grass scenarios, respectively.

The impact of small predicted increases in the 2050 MMSEA precipitation in July and October on monthly surface runoff was negligible (Fig. 4c). Surface soil moisture, however, increased in most months, particularly July and August (Fig. 4d). The extreme scenarios reduced surface runoff in all months. The irrigated-crop scenario produced a negative value for surface runoff in moderately dry October—by definition in the model, the water necessary to maintain wet soil conditions for this vegetation type was obtained through reducing surface runoff (Fig. 4d). In contrast, the short-grass scenario reduced surface-layer water content substantially, because roots of this land cover type are in the simulated surface soil layer.

Linking projected 2050 changes in MMSEA LCLU to the changes in precipitation requires consideration of the effects on other surface water and energy variables, such as latent and sensible heat flux, specific humidity and air temperature. For northern MMSEA region, the control simulation indicates that most of the available surface energy is partitioned into latent heat flux, which exhibits small monthly variation (~124 Wm^{-2}) until October when reduced to 93 Wm^{-2} (Fig. 4e). The simulated 2050 LCLU scenario shows only a slight increase in July and August latent heat flux. In contrast, the irrigated-crop scenario increased latent heat flux in all months; the short-grass scenario decreased it. Absolute changes are larger in the grass versus irrigated-crop scenario. The projected 2050 LCLU scenario reduced sensible heat flux slightly in all months, with the largest changes occurring in July and August (Fig. 4f). The irrigated crop scenario decreased sensible heat flux, while the grass scenario increased it in all months. Irrigation reduced variability in both sensible and latent heat flux.

Changes in surface heat flux influence near surface-meteorological variables such as air temperature and specific humidity. Consistent with the increases in latent heat flux, the projected 2050 LCLU scenario increases the July and August specific humidity slightly (Fig. 4g). Specific humidity increases in all months in response to conversion to irrigated crops; but the opposite occurs in the short-grass scenario. The response of surface air temperature to the projected 2050 LCLU scenario is also marginal (Fig. 4h). Monthly reductions are seen in all months, with those in July and August being the largest. The irrigated-crop scenario decreased surface air temperature while the short-grass scenario increased it. Changes in some other surface variables are given in Online Resource 3.

Simulated changes in surface meteorological variables affect atmospheric variables at the lower layers of the troposphere, for example the 850 hPa level. For the projected 2050 LCLU scenario, the changes in the JJA specific humidity were usually small (less than 0.1 g kg^{-1}) across the domain (Fig. 5a). Nevertheless, an increase was usually found over northern MMSEA, while a decrease was seen over the central southern China. Changes in wind magnitude were generally small (Fig. 5b). However, the wind magnitude over MMSEA weakened slightly, indicating a weakening of the monsoonal flow. The irrigated-crop scenario increased humidity in the 850 hPa level over northern MMSEA (Fig. 5c). Specific humidity also increased over the Bay of Bengal and the northern South China Sea; but it was reduced over south and central eastern China. The same scenario enhanced the wind strength over the MMSEA (Fig. 5d), most likely a result of the significant reduction in the roughness length (Table 1). This change caused an anticyclone-like anomaly in the

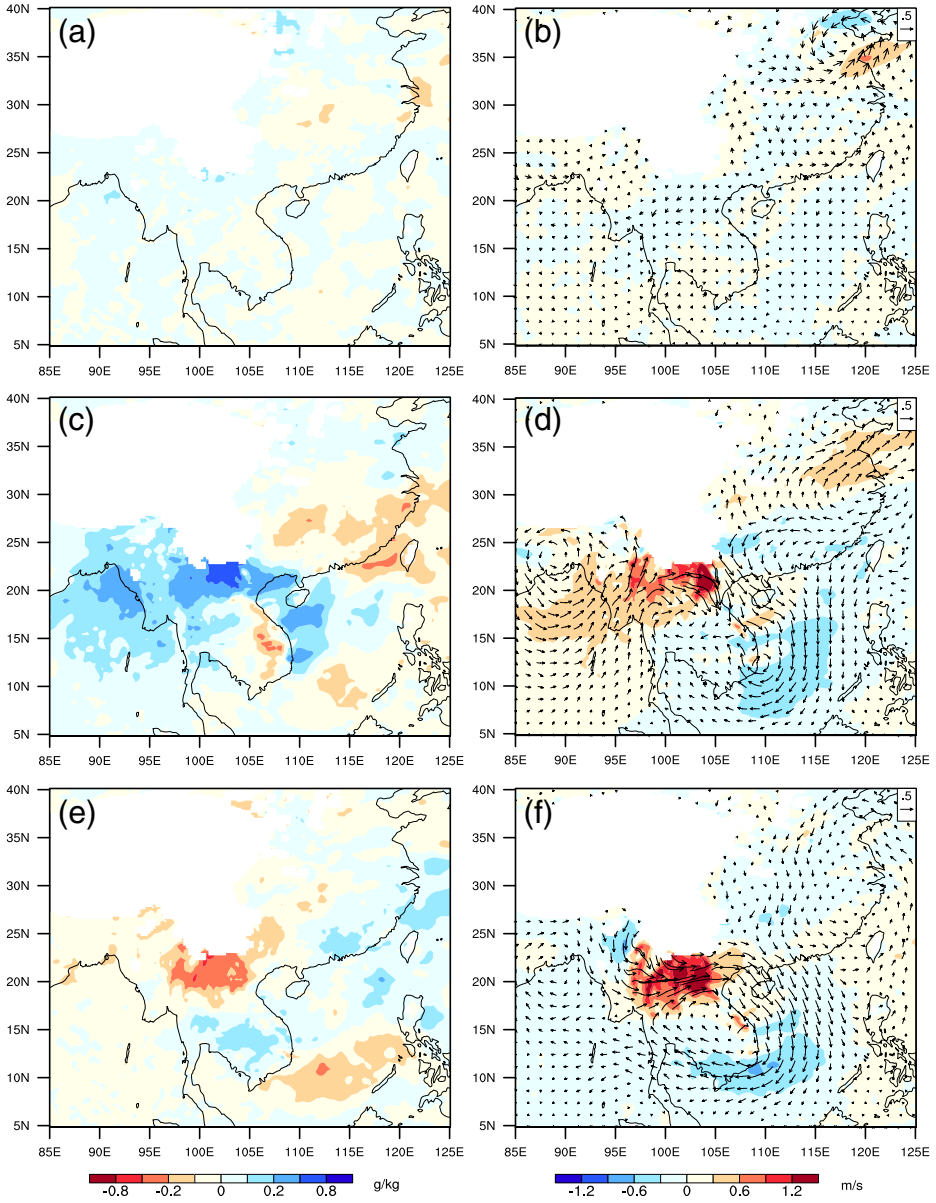

Fig. 5 JJA changes in 850 hPa specific humidity (plots on the left side) and wind vectors and magnitude (plots on the right side): **a** and **b** for 2050 LCLU, **c** and **d** for irrigated crop scenario, and (**e**) and (**f**) for short grass scenario

wind fields over IP and South China Sea. Such an anomaly means that the monsoonal flow is strengthened over MMSEA while weakened over South China Sea. In addition, the irrigated-crop scenario enhanced the winds over the northern sections of southern China, but weakened them over the rest of southern China. The short-grass scenario reduced the 850 hPa-level specific humidity over northern MMSEA, but it yielded increases over

southern IP and southern China (Fig. 5e). The changes in the wind fields over IP and South China Sea are similar to those in the irrigated-crop scenario (Fig. 5f). Nonetheless, the magnitudes of the changes in the short-grass scenario were greater. Both reference scenarios generate important changes in the atmospheric fields and circulation over Southeast Asia; and these changes lead to corresponding changes in the regional precipitation (Fig. 3). Changes in 700-hPa and 500-hPa fields are similarly provided in Online Resource 4 and 5, respectively.

4 Discussion

The projected 2050 LCLU scenario did not change regional precipitation greatly compared with the extreme deforestation scenarios. Two factors may have contributed to this outcome: the extent and spatial heterogeneity of the predicted LCLU patterns, and the type of forest conversion. The projected 2050 LCLU changes, although substantial, are distributed throughout the MMSEA region, but not necessarily arranged in large contiguous blocks. The upscaling process from the 0.926-km land-cover map to the 9.26-km model resolution using the dominant cover approach likely eliminated many smaller, isolated patches of various land covers. The LCLU change at 9.26-km resolution was about 11 %, lower than the 16 % projected at the finer scale. In addition, some of the predicted forest conversion reflects changes from one woody vegetation type to another. In such cases the changes in surface parameters that determine the interaction between surface and atmosphere are smaller than those for the conversion to a crops or grass; and therefore, may limit the effect of predicted forest transitions in MMSEA on regional climate.

Extreme LCLU scenario simulations are used to provide information about the boundaries of climatic response to landscape perturbations, fostering better understanding of how tropical forest biomes affect the climate system (e.g., Nobre et al. 1991; Kanae et al. 2001; Sen et al. 2004; Silva et al. 2006; Schneck and Mosbrugger 2011). The local climatic responses to the extreme scenario perturbations in our study were generally similar to those reported by others, despite the dominance of the external monsoonal forcing. Replacing forest with irrigated crop tended to increase precipitation, whereas replacing forest with short grass tended to decrease it. In addition to the local effects of Southeast Asian deforestation, some studies report strong teleconnections to the extratropical as well as tropical regions (e.g., Werth and Avissar 2005; Schneck and Mosbrugger 2011). In these studies, the propagation of the signal, which is in the form of sensible heat, potential energy and geopotential changes, is associated with the high-level wind circulation. In our study, the extreme deforestation scenario simulations also impacted areas remote from perturbed MMSEA. The irrigated-crop perturbation impacted rainfall more in downwind areas than did the short-grass perturbation because of a fundamental difference between these two vegetation types in the model. Unlike short grass, vegetation in the irrigated crop scenario is never subject to soil moisture stress, a condition that could help sustain higher transpiration rates. The high rates of latent heat flux also confirm the latter (Fig. 4e). Irrigated-crop vegetation transfers more water vapor and energy in the form of latent heat to the overlying atmosphere. Given that the winds are modified in a similar way in both extreme scenarios (i.e., strengthened over the perturbation area while weakened over South China Sea), the major remote differences likely arise as a result of the content (humidity and energy) change in the strong monsoonal flow.

5 Conclusions

Much of the uncertainty in attempting to understand the hydrological impacts of tropical deforestation stems from a failure to use realistic LCLU projections in climate simulations (Giambelluca et al. 1996). While extreme deforestation scenarios have often been used to explore the realm of possible changes, realistic change scenarios have been uncommon. Our simulations showed that while extreme cases of deforestation produced substantial changes in regional precipitation over the model domain including the Indochina Peninsula, southern China, and the South China Sea, simulations of a plausible 2050 LCLU scenario produce little change in precipitation or other important hydro-climatological variables. The results imply that greenhouse gas emissions may have larger impact on the climate of the region than land-cover change. However, while the 16 % change we simulated was based on the most recent, credible forecast of land cover change in the region, it did not incorporate potential LCLU changes in lowland areas, and some change was lost in up-scaling from map to model resolution. Nevertheless, the study provides a reference LCLU change simulation for the MMSEA region to compare with the results of the climate change simulations involving greenhouse gas emission scenarios. Future simulations should aim to integrate even more realistic LCLU change projections, rather than relying on extreme cases of deforestation.

Acknowledgments This work was supported by NASA (#NNG04GH59G) and APN (ARCP2007-01CMY).

References

Castro CL, Pielke RA Sr, Leoncini G (2005) Dynamical downscaling: assessment of value retained and added using the Regional Atmospheric Modeling System (RAMS). J Geophys Res 110:D05108. doi:10.1029/2004JDD004721

Chen W, Jiang Z, Li L, Yiou P (2011) Simulation of regional climate change under the IPCC A2 scenario in southeast China. Clim Dyn 36:491–507

Chotamonsak C, Salathe EP Jr, Kreasuwan J, Chantara S, Siriwitayakorn K (2011) Projected climate change over Southeast Asia simulated using a WRF regional climate model. Atmos Sci Let 12:213–219

Chow KC, Chan JCL, Pal JS, Giorgi F (2006) Convection suppression criteria applied to the MIT cumulus parameterization scheme for simulating the Asian summer monsoon. Geophys Res Lett 33:L24709. doi:10.1029/2006GL028026

Dickinson RE, Henderson-Sellers A, Kennedy PJ (1993) Biosphere-atmosphere transfer scheme (bats) version 1e as coupled to the NCAR community climate model. Tech. rep., National Center for Atmospheric Research, Colorado

FAO (2010) The global forest resource assessment. FAO, Rome

Foley JA, Levis S, Prentice IC, Pollard D, Thompson SL (1998) Coupling dynamic models of climate and vegetation. Glob Change Biol 4:561–579

Fox JM, Vogler JB, Sen OL, Ziegler AD, Giambelluca TW (2012) Simulating land-cover change in Montane Mainland Southeast Asia. Environ Manage 49(5):968–979

Gao XJ, Shi Y, Zhang DF, Wu J, Giorgi F, Ji ZM, Wang YG (2012) Uncertainties of monsoon precipitation projection over China: results from two high resolution RCM simulations. Clim Res 52:213–226. doi:10.3354/cr01084

Giambelluca TW, Tran LT, Ziegler AD, Menard TP, Nullet MA (1996) Soil-vegetation-atmosphere processes: simulation and field measurement for deforested sites in northern Thailand. J Geophys Res Atmos 101:25,867–25,885

Giambelluca TW, Ziegler AD, Nullet MA, Dao TM, Tran LT (2003) Transpiration in a small tropical forest patch. Ag Forest Meteorol 117:1–22

Giorgi F, Francisco R, Pal JS (2003) Effects of a subgrid-scale topography and land use scheme on the simulation of surface climate and hydrology. Part 1: effects of temperature and water vapor disaggregation. J Hydromet 4:317–333

Grell G (1993) Prognostic evaluation of assumptions used by cumulus parameterizations. Mon Wea Rev 121:764–787

Guardiola-Claramonte M, Troch PA, Ziegler AD, Giambelluca TW, Durcik M, Vogler JB, Nullet MA (2010) Modeling basin-scale hydrologic effects of rubber (Hevea brasiliensis) in a tropical catchment. Ecohydrology 3(3):306–314

Holtslag AAM, de Bruijn EIF, Pan H-L (1990) A high resolution air mass transformation model for short-range weather forecasting. Mon Wea Rev 118:1561–1575

Hsie EY, Anthes RA, Keyser D (1984) Numerical simulation of frontogenesis in a moist atmosphere. J Atmos Sci 41:2581–2594

Kanae S, Oki T, Musiake K (2001) Impact of deforestation on regional precipitation over the Indochina Peninsula. J Hydrometeor 2:51–70

Karl TR, Trenberth KE (2003) Modern global climate change. Science 302:1719–1723

Kiehl JT, Hack JJ, Bonan GB, Boville BA, Breigleb BP, Williamson D, Rasch P (1996) Description of the NCAR community climate model (CCM3). Tech. Rep. NCAR/TN-420 + STR. National Center for Atmospheric Research

Nobre CA, Sellers PJ, Shukla J (1991) Amazonian deforestation and regional climate change. J Climate 4:957–988

Pal J, Small E, Eltahir E (2000) Simulation of regional-scale water and energy budgets: representation of subgrid cloud and precipitation processes within regcm. J Geophys Res-Atmos 105(D24):29579–29594

Pal JS, Giorgi F, Bi XQ, Elguindi N et al (2007) Regional climate modeling for the developing world: the ICTP RegCM3 and RegCNET. Bull Am Meteorol Soc 88:1395–1409

Pielke RA Sr, Adegoke J, Beltran-Przekurat A, Hiemstra CA, Lin J, Nair US, Niyogi D, Nobis TE (2007) An overview of regional land-use and land-cover impacts on rainfall. Tellus 59B:587–590

Schneck R, Mosbrugger V (2011) Simulated climate effects of Southeast Asian deforestation: regional processes and teleconnection mechanisms. J Geophys Res 116:D11116. doi:10.1029/2010JD015450

Segal M, Pan Z, Turner RW, Takle ES (1998) On the potential impact of irrigated areas in North America summer rainfall caused by large-scale systems. J Appl Meteor 37:325–331

Sen OL, Wang Y, Wang B (2004) Impact of Indochina deforestation on the East-Asian summer monsoon. J Clim 17:1366–1380

Sen OL, Bozkurt D, Fox JM, Vogler JB, Giambelluca TW, Ziegler AD (2012) Projected impacts of global warming on regional climate in southeast Asia. Clim Dyn (forthcoming)

Silva MES, Franchito SH, Rao VB (2006) Effects of Amazonian deforestation on climate: a numerical experiment with a coupled biosphere-atmosphere model with soil hydrology. Theoret Appl Clim 85:1–18

Wang Y, Sen OL, Wang B (2003) A highly resolved regional climate model (IPRC_RegCM) and its simulation of the 1998 severe precipitation event over China. Part I: model description and control experiment. J Climate 16:1721–1738

Wang Y, Leung LR, McGregor JL, Lee DK, Wang WC, Ding Y, Kimura F (2004) Regional climate modeling: progress, challenges, and prospects. J Meteorol Soc Jpn 82(6):1599–1628

Werth D, Avissar R (2005) The local and global effects of Southeast Asian deforestation. Geophys Res Lett 32:L20702. doi:10.1029/2005GL022970

Xie P, Arkin PA (1997) Global precipitation: A 17-year monthly analysis based on gauge observations, satellite estimates, and numerical model outputs. Bull Amer Meteor Soc 78:2539–2558

Yatagai A, Kamiguchi K, Arakawa O, Hamada A, Yasutomi N, Kitoh A (2012) APHRODITE: constructing a long-term daily gridded precipitation dataset for Asia based on a dense network of rain gauges. Bull Am Meteorol Soc. doi:10.1175/BAMS-D-11-00122.1

Zeng X, Zhao M, Dickinson RE (1998) Intercomparison of bulk aerodynamic algorithms for the computation of sea surface fluxes using TOGA COARE and TAO data. J Climate 11:2628–2644

Zhang DF, Gao XJ, Ouyang LC (2008) Simulation of present climate over China by a regional climate model. J Trop Meteorol 14(1):19–23

Ziegler AD, Fox JM, Xu JC (2009a) The rubber juggernaut. Science 324:1024–1025

Ziegler AD, Bruun TB, Guardiola-Claramonte M, Giambelluca TW, Lawrence D, Lam NT (2009b) Environmental consequences of the demise in Swidden agriculture in SE Asia: geomorphological processes. Human Ecol 37:361–373